Historical Biology
An International Journal of Paleobiology

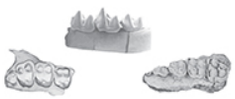

Taylor & Francis
Taylor & Francis Group

Historical Biology
An International Journal of Paleobiology

ISSN: (Print) (Online) Journal homepage: https://www.tandfonline.com/loi/ghbi20

Biting in the Miocene seas: estimation of the bite force of the macroraptorial sperm whale *Zygophyseter varolai* using finite element analysis

Emanuele Peri, Peter L. Falkingham, Alberto Collareta & Giovanni Bianucci

To cite this article: Emanuele Peri, Peter L. Falkingham, Alberto Collareta & Giovanni Bianucci (2022) Biting in the Miocene seas: estimation of the bite force of the macroraptorial sperm whale *Zygophyseter varolai* using finite element analysis, Historical Biology, 34:10, 1916-1927, DOI: 10.1080/08912963.2021.1986814

To link to this article: https://doi.org/10.1080/08912963.2021.1986814

Published online: 20 Oct 2021.

HISTORICAL BIOLOGY
2022, VOL. 34, NO. 10, 1916–1927
https://doi.org/10.1080/08912963.2021.1986814

Taylor & Francis
Taylor & Francis Group

Biting in the Miocene seas: estimation of the bite force of the macroraptorial sperm whale *Zygophyseter varolai* using finite element analysis

Emanuele Peri [a,b,c], Peter L. Falkingham [b], Alberto Collareta [c] and Giovanni Bianucci [c]

[a]Dottorato Regionale Pegaso in Scienze Della Terra, Università Di Pisa, Pisa, Italy; [b]School of Biological and Environmental Sciences, Liverpool John Moores University, Liverpool, UK; [c]Dipartimento Scienze Della Terra, Università Degli Studi Di Pisa, Pisa, Italy

ABSTRACT

Differing from the extant physeteroids, macroraptorial sperm whales are currently regarded as apex predators of the Miocene seas based on several morphofunctional observations. Here, we estimate the bite force of *Zygophyseter varolai*, a macroraptorial physeteroid from lower upper Miocene strata of the Pietra leccese formation (Apulia, Italy) using the finite element analysis (FEA). To explore multiple bite scenarios, we set four different load cases on a 3D model of the cranium obtained via digital photogrammetry, considering the temporalis and masseter muscles as jaw adductors. Our FEA simulations indicate that *Z. varolai* exerted an anterior bite force of more than 4000 N and a posterior bite force of more than 10000 N. These values are similar to those estimated for other marine predators known for their powerful bite. This suggests that *Z. varolai* might have fed upon medium-sized marine vertebrates like other odontocetes. Considering the significant difference observed between the anterior and posterior bite forces, *Z. varolai* likely fed via 'grip-and-shear' feeding, snapping the food items with an anterior bite and then cutting them with a powerful posterior bite. Other macroraptorial sperm whales such as the roughly coeval *Acrophyseter* from Peru likely employed the same feeding technique.

ARTICLE HISTORY
Received 20 August 2021
Accepted 20 September 2021

KEYWORDS
Physeteroidea; apex predator; biomechanics; FEA; feeding strategy; palaeoecology

Introduction

Since the earliest predator–prey interaction, oceans have always had their sea monsters. Once jaws had evolved, bite force became a defining characteristic of predators. During the Late Devonian, the top predator of the seas was the placoderm *Dunkleosteus*, an armoured, jawed fish more than 8 m long, and calculated to have had a bite force of 7495 N at the rear gnathal plates (Anderson and Westneat 2009; Ferrón et al. 2017). From the late Triassic to the late Cretaceous, the role of marine apex predators was mainly played by marine reptiles such as the Pliosauroidea (Plesiosauria, Sauropterygia) (Foffa et al. 2014). Pliosauroids included large-sized predators like *Kronosaurus queenslandicus*, with a total body length of 9–10.9 m and an estimated bite force of more than 27000 N (McHenry 2009; Foffa et al. 2014). Near the end of the Cretaceous period (98–65.5 Ma), Mosasauroidea (Squamata) roamed the seas together with Pliosauroidea and ruled the aquatic environments till the end of the Mesozoic (Polcyn et al. 2014; Madzia and Cau 2017). Mosasauroids were marine reptiles with a lacertiform appearance, and the largest species exceeded 10 m in length (Bullard and Caldwell 2010; Driscoll et al. 2019). After the K-Pg boundary, during the Palaeocene and part of the Eocene, the role of apex predator in oceans was still occupied by reptiles, with large marine crocodiles like the genera *Thoracosaurus* (Danian, Palaeocene) and *Dyrosaurus* (Ypresian, Eocene) (Gallagher 2003; Jouve et al. 2005; Puértolas-Pascual et al. 2015). Besides crocodiles, the selachian family Otodontidae provided important marine predators in the Palaeogene with the megatoothed shark species *Otodus obliquus* (Palaeocene) and *Carcharocles auriculatus* (Eocene) (Ehret and Ebersole 2014; Perez et al. 2018). From the middle Eocene, marine mammals became the new top predators in seas thanks to the radiation of the Archaeoceti (Fordyce 2018; Uhen 2018). This group includes some of the most impressive fossil marine predators like *Basilosaurus* (Basilosauridae), a huge archaic whale (total body length 17–20 m) with serrated teeth and a bone-crushing bite (Snively et al. 2015; Uhen 2018; Voss et al. 2019). Near the end of the Eocene, cetaceans radiated into the modern Mysticeti and Odontoceti lineages (forming the Neoceti clade) and new predator taxa with various morphologies and feeding strategies occupied the top of the trophic chain (Boessenecker et al. 2020). Nowadays, the cetacean apex predator is the killer whale (*Orcinus orca*; Delphinidae, Odontoceti), which thanks to its large size and coordinated hunting strategies can feed upon sperm whales as well as large baleen whales (mysticetes) like common minke whales (*Balaenoptera acutorostrata*), calves of humpback whales (*Megaptera novaeangliae*), and grey whales (*Eschrichtius robustus*) (Pitman et al. 2001, 2015; Barrett-Lennard et al. 2011; Ford 2018). In modern oceans, the killer whale shares the top position of the trophic chains with the great white shark (*Carcharodon carcharias*), whose predatory activity on diminutive marine mammals is widely known (Compagno 1984; Heithaus 2001; Brown et al. 2010; Skomal et al. 2017; Moro et al. 2020).

In the Miocene epoch, sharks belonging to the family Otodontidae roamed the oceans covering the ecological role of apex predators (Ehret and Ebersole 2014; Collareta et al. 2017a; Perez et al. 2018; Boessenecker et al. 2019). *Carcharocles megalodon* (total body length up to 20 m; Perez et al. 2021) was the most impressive representative of the otodontid family, and it likely fed upon small to medium-sized baleen whales (Collareta et al. 2017a; Boessenecker et al. 2019; Cooper et al. 2020; Shimada et al. 2020). During the same epoch, high trophic levels of predation like those of the modern killer whale have been proposed for some fossil

CONTACT Emanuele Peri emanuele.peri@phd.unipi.it Dottorato Regionale Pegaso in Scienze Della Terra, Università Di Pisa, Via S. Maria 53, Pisa 56126, Italy

Published online 20 Oct 2021

relatives of the modern sperm whales (superfamily Physeteroidea) (Bianucci and Landini 2006; Lambert et al. 2008, 2010, 2017). Differently from the extant physetheroids (i.e., the sperm whale *Physeter macrocephalus*, the dwarf sperm whale *Kogia sima*, and the pygmy sperm whale *K. breviceps*), which feed nearly exclusively upon cephalopods by suction generated through the mouth in *Kogia* and directly within the oropharynx in *Physeter* (Werth 2004, 2006a, 2006b; Bloodworth and Marshall 2005), these putatively macroraptorial, extinct forms likely preyed upon marine vertebrates using robust jaws and large teeth to grasp their food items (Bianucci and Landini 2006; Lambert et al. 2008, 2010, 2014, 2017; Hocking et al. 2017; Lambert and Bianucci 2019; Peri et al. 2020). This hypothesis is based on various cranial features displayed by the macroraptorial Physeteroidea, including a wide temporal fossa, well-developed maxillary teeth (only mandibular teeth are functional in extant sperm whales) and, as observed on the holotype of *Acrophyseter robustus*, bony exostoses in correspondence of upper cheek teeth (Bianucci and Landini 2006; Lambert et al. 2008, 2010, 2014; Lambert and Bianucci 2019; Peri et al. 2020). Furthermore, the teeth of these fossil sperm whales exhibit deep occlusal facets, which are sulci on the tooth surface produced by repeated tooth-to-tooth contacts (attritional wear), and fractures attributed to strong occlusion or to the contact with hard material (e.g., bone) (Bianucci and Landini 2006; Lambert et al. 2017; Lambert and Bianucci 2019; Peri et al. 2020). Taxonomically diagnostic fossil remains of macroraptorial physeteroids have been retrieved in several localities all around the world, both in the middle Miocene (*Albicetus oxymycterus*, California, USA; *Brygmophyseter shigensis*, Japan) and in the upper Miocene (*Acrophyseter deinodon, Acrophyseter robustus* and *Livyatan melvillei*, Peru; *Zygophyseter varolai*, Italy) (Bianucci and Landini 2006; Kimura et al. 2006; Lambert et al. 2008, 2010, 2017; Boersma and Pyenson 2015). One of the best known macroraptorial physeteroids, *Z. varolai* from Tortonian strata of the Pietra leccese formation (Salento Peninsula, southern Italy), is characterised by having a dorsal concavity on the skull (i.e., supracranial basin) that is wide and hemispherical, an extremely elongated zygomatic process (probably supporting a developed masseter muscle), and several dental features associated to a strong occlusion and repetitive use of the bite (e.g. occlusal facets, lowering of the gingival collar due to the deepening of the associate occlusal facet, and lateral wear of the enamel layer) (Bianucci and Landini 2006). The holotype of *Z. varolai* is complete enough to provide reliable estimations of both the condylobasal length (148 cm) and the total body length (650–700 cm). All these elements led to the hypothesis that *Z. varolai* preyed upon small- to medium-sized marine vertebrates using a powerful bite (Bianucci and Landini 2006).

Here, we use the 'dry-skull' method and the finite element analysis (FEA) to estimate the bite force of *Z. varolai* and test the bite performances of this extinct macroraptorial sperm whale. FEA has proven to be a powerful tool to investigate form and function of extinct vertebrates (Rayfield et al. 2001; Hassan et al. 2002; McHenry et al. 2007; Wroe et al. 2007; Bell et al. 2009; Oldfield et al. 2012; Foffa et al. 2014; Snively et al. 2015), but such a biomechanical approach has never been used before on a macroraptorial sperm whale. The results obtained from the FEA bite simulations provide informative clues about the palaeoecology of this top predator from the late Miocene, and open new intriguing research horizons concerning the macroraptorial physeteroids and their trophic role in the Miocene global ocean.

Materials and methods

Institutional abbreviations

MAUS, Museo dell'Ambiente, Università del Salento, Lecce, Italy; MNHN, Muséum National d'Histoire Naturelle, Paris, France; MSNUP, Museo di Storia Naturale dell'Università di Pisa, Calci, Italy; MUSM, Museo de Historia Natural, Universidad Nacional Mayor de San Marcos, Lima, Peru.

Examined specimen

The specimen used in this study is a cast of the cranium and the mandibles of the holotype of *Zygophyseter varolai* (MSNUP I-16828). The holotype (MAUS 229, a replacement number for MAUL 229/1 reported in Bianucci and Landini 2006) also includes most of the postcrania and was collected from the uppermost strata of the Cisterna quarry of Salento peninsula (Lecce Province, southern Italy) (Bianucci and Landini 2006; Bianucci and Varola 2014). The cranium lacks the right lacrimo-jugal complex and the posterodorsal portion of the supracranial basin. These cranial parts were included in stone slabs that were not collected from the quarry (the right lacrimo-jugal complex) or were lost before the fossil could be stored at the MAUS (the posterodorsal portion of the supracranial basin). The mandibles are virtually complete, although the right coronoid process appears slightly deformed.

Digital acquisition

We acquired a 3D model of the cranium and mandibles of *Z. varolai* through digital photogrammetry of the holotype cast accomplished with the software Agisoft Metashape (1.7.0) (Petti et al. 2008; Falkingham 2012; Falkingham et al. 2014, 2018, 2020; Mallison and Wings 2014; Fahlke and Autenrieth 2016; Fau et al. 2016; Díez Díaz et al. 2021). The camera used for the photographic acquisition was a Sony a6000 equipped with a Sigma 30 mm F1.4 lens. We performed two separate acquisitions for the cranium (94 photos) and the mandibles (134 photos). To reconstruct the missing parts, we imported the digital model of the cranium into Blender (2.91.0) (https://www.blender.org/) and digitally rebuilt the posterodorsal portion of the cranium and the missing right lacrimojugal complex. Our reconstruction of the missing posterodorsal portion of the cranium was based on observations made in the quarry during the collection of the fossil by one of us (G.B.) as well as on comparisons with the holotypes of *Acrophyseter deinodon* (MNHN SAS 1626) and *Acrophyseter robustus* (MUSM 1399) (which, among the physeteroid species, are the phylogenetically and morphologically closest to *Zygophyseter* according to Lambert et al. 2017). The missing right lacrimojugal complex was digitally rebuilt by mirroring its well-preserved left antimere. Concerning the 3D mesh of the mandibles, we retrodeformed the right coronoid process in Blender in light of careful comparations with the substantially undeformed left coronoid process. Since we acquired both the 3D model of the cranium and of the mandible by digital photogrammetry, the internal geometry of the *Z. varolai* skull is missing. The only way to obtain the internal geometry of a vertebrate skull is via computed axial tomography (CT scan). However, we used digital photogrammetry here because moving the holotype specimen would have seriously threatened its integrity; moreover, the large size and weight of the *Z. varolai* skull would have made the acquisition through conventional CT scans very difficult. Although the lack of the internal cranial geometry may affect the results of biomechanical simulations, previous studies have demonstrated that surface meshes and simplified 3D geometries can provide reliable

estimations of reaction forces associated with biting actions (which are the focus of the present work) and allow for general analyses of stress distribution (Rayfield et al. 2007; Snively et al. 2015).

Reconstruction of the muscles

To estimate the bite force of *Z. varolai* we followed the methods proposed by Snively et al. (2015) for investigating the bite of *Basilosaurus isis*: the bite was considered static, where the velocity of muscles is 0 m/s and exerting isometric force. In this condition, the muscle force is equal to the anatomical cross-section of the muscle multiplied by the specific muscular tension. In several studies, the specific tension of the mammalian musculature has been set to 30 N/cm^2 (e.g., Weijs and Hillen 1985; Thomason 1991; Wroe et al. 2005; Snively et al. 2015); however, factors like the pennation of the muscle and changes in the fibre length could increase this value (Koolstra et al. 1988; Wroe et al. 2005; McHenry et al. 2007; Snively et al. 2015). Considering the significant pennation of the mammalian temporalis muscle as well as the available data in literature on the muscular anatomy of extant odontocetes (Von Schulte and De Forest Smith 1918; Seagars 1982), in our model we considered a specific muscular tension value of 37 N/cm^2, as already done elsewhere (Christiansen 2007; Snively et al. 2015).

In order to estimate the anatomical cross-section of the temporalis muscle, we used the 'dry-skull' method (Thomason 1991): in the Blender workspace, we modelled a polygon having the shape of the area described by the zygomatic arch (which is defined by the zygomatic process of the squamosal and lacrimo-jugal complex) and the lateral wall of the temporal fossa as appearing in ventral view. Considering the strong asymmetry that affects the cranium of physeteroids (Bianucci and Landini 2006; Lambert et al. 2017, 2020; Collareta et al. 2020b), we repeated the process on both the right and left sides of the skull. The cross-section of the masseter was harder to estimate than that of the temporalis, due to the lack of clear bony constraints for this muscle. Following what was done by Snively et al. (2015) in their study about the bite force of *Basilosaurus isis*, we assumed the cross-section of the masseter to be equal to 10% of that of the temporalis. To substantiate this assumption, we observed that both *Z. varolai* and *B. isis* display a wide cross-section of the temporalis muscle and elongated zygomatic arches (Bianucci and Landini 2006; Snively et al. 2015). This is apparent by studying the ratio between the length of the zygomatic arch and the distance measured from the tip of the rostrum to the posteriormost point of the temporal fossa: this ratio equals 0.28 in *B. isis*, 0.20 in *Z. varolai*, and 0.06 in *Physeter macrocephalus*. Such values indicate that *B. isis* and *Z. varolai* bear similarly elongated zygomatic arches, thus greatly differing from *P. macrocephalus* in this respect. Based on these considerations, the assumption of a cross-section area of the masseter equalling 10% of that of the temporalis is here regarded as reasonable for *Z. varolai*. Subsequently, we digitally coupled the skull with the mandibles in Blender and determined the direction of the muscular vectors. We calculated the latter at two mouth gape angles (20° and 35°) in order to estimate the bite force exerted on different bite scenarios. We chose such gape angles as they were selected for carrying out the FEA analyses on *B. isis* (ca. 20°, measured from Snively et al. 2015: Figure 1a) and *Carcharodon carcharias* (35°; Wroe et al. 2008), thus allowing for robust comparisons of bite force values in these marine predator species. As origin of the temporalis muscle, we chose the entire surface of the temporal fossa (Figure 1), following the reconstruction proposed by Lambert et al. (2014) for *Acrophyseter robustus* and the muscular anatomy of extant odontocetes (Von Schulte and De Forest Smith 1918; Seagars 1982).

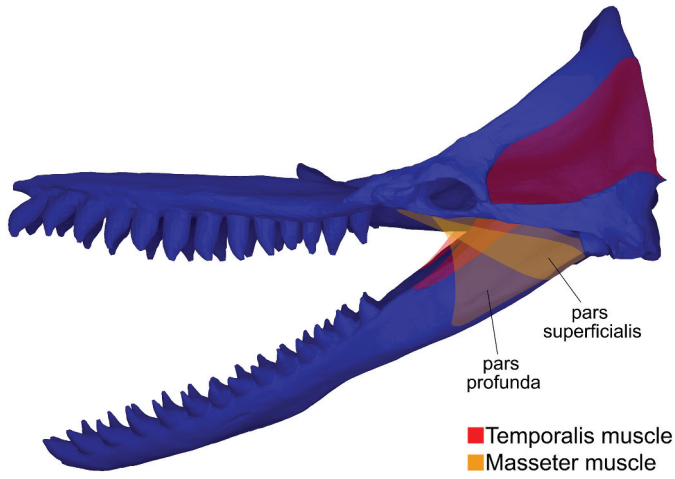

Figure 1. Reconstruction of the *Zygophyseter varolai* skull and mandibles in lateral view, based on the cast of the holotype (MSNUP I-16828), and schematic reconstruction of the temporalis (red) and masseter (including the pars superficialis and pars profunda) (yellow).

Concerning the masseter muscle, we placed the origin of the pars superficialis on the lacrimo-jugal complex, whereas the origin of the pars profunda was reconstructed as distributed between the lacrimo-jugal complex and the zygomatic process (Figure 1) (Von Schulte and De Forest Smith 1918; Seagars 1982). *Zygophyseter varolai* displays a keel along the anterior crest of the coronoid process that we tentatively interpreted as marking the anterior limit of the temporalis muscle insertion. We based our reconstruction of the masseter insertion on the observation of a low but well-defined crest paralleling the ventral margin of the mandible and projecting anteriorly from the mandibular condyle. Moreover, to rebuild the masseter architecture of *Z. varolai*, we also followed previous reconstructions for the holotype of *A. deinodon* (MNHN SAS 1626) and anatomical data from extant odontocetes (Von Schulte and De Forest Smith 1918; Seagars 1982; Lambert et al. 2008, 2017).

Simulating a biting action in a fossil mammal can prove a challenging task: one of the most crucial phases is reconstructing the jaw adduction muscle architecture of the species under examination. However, muscles are soft tissues that are only rarely preserved in the fossil record; thus, researchers often base their assumptions on soft-tissue anatomical data from extant taxa (which are often quite rare in literature). Therefore, a future development of physiological and anatomical studies aimed at increasing our knowledge of muscle architecture and its functions in living taxa is desirable (Bates and Falkingham 2018). In a mammalian biting action, at least three muscular groups are involved: temporalis, masseter, and pterygoid (Weijs 1985; Thomason 1991). For our purposes, we did not estimate any force for the pterygoid because, in mammals, the contribution of this muscle group to the mandible adduction can be regarded as irrelevant (Snively et al. 2015).

Simulating a bite

We used the software GOM Inspect 2019 (https://www.gom.com/it/software-3d.html) to reduce the polygon count and to optimise the topology of the high-density photogrammetry mesh into a cleaner, smaller mesh appropriate for FEA. The final result was a 3D. stl model of the *Zygophyseter* cranium having 10000 vertices and 20008 faces (Figure 1). To perform the bite simulations, we used Autodesk Inventor 2020 (https://www.autodesk.it/products/

inventor/overview), the finite element (FE) solver of the Autodesk suite. In Autodesk Inventor, the model was converted to a FE mesh consisting of 100076 nodes and 60327 elements. We set the material as isotropic, and trade-off values between the mammalian compact bone and dentine were adopted to describe the elastic behaviour of the *Z. varolai* cranium (elastic modulus E = 17.4 GPa and Poisson's ratio = 0.34) (Martin et al. 2015; Snively et al. 2015). Concerning the volumetric density, we assigned a value (1.38 gr/cm^3) averaging the density of the maxilla and occipital in the common dolphin (*Delphinus delphis*) (de Buffrénil and Sire J-Y 1986). It is worth mentioning here that the cranium of the extant sperm whale *P. macrocephalus* displays an amphitheatre-shaped supracranial basin formed by a macroporous lamina between two denser bony layers (Alam et al. 2016). Such a peculiar osteoanatomical structure likely results in a lower bone density compared to other toothed whales. However, based on the observation of broken bone surfaces in the holotypes of *Z. varolai* and *A. deinodon*, we contend that macroraptorial sperm whales did not display a macroporous lamina.

To simulate the mandibular joints, we placed a fixed constraint on each squamosal at level of the mandibular fossa; in addition, a third fixed constraint was placed alternatively on the posteriormost and anteriormost upper left teeth, thus simulating the resistance of a food item during posterior and anterior biting actions, respectively. The reaction force generated at the dental constraint represents the bite force exerted in that specific point (following Snively et al. 2015). Varying the position of the dental constraint and the gape angle of the mouth, we made four simulations corresponding to four load cases:

- 20° gape angle, constraint at the anteriormost teeth (anterior bite)
- 20° gape angle, constraint at the posteriormost tooth (posterior bite)
- 35° gape angle, constraint at the anteriormost tooth (anterior bite)
- 35° gape angle, constraint at the posteriormost tooth (posterior bite)

Finally, we compared the von Mises stress patterns obtained for the four loading cases, to explore how stress distribution varies during an anterior and posterior biting actions.

Comparative palaeoecology

In order to compare the bite force of *Z. varolai* with that exerted by an extant marine apex predator in a comparative palaeoecological framework, we estimated the body mass of a hypothetical great white shark (*Carcharodon carcharias*) that could generate the same bite forces estimated for *Zygophyseter* at 35° gape angle by following the equation proposed by Wroe et al. (2008). Furthermore, we applied the equation provided by Kohler et al. (1996) to calculate the total length of such a hypothetical great white shark. We did not perform this calculation for the bite force at 20° gape angle because Wroe et al. (2008) proposed their bite force estimation at a gape angle of 35°. Consequently, doing the same calculation with the *Z. varolai* bite force at 20° would produce misleading data.

Results

The bite force results obtained from our FE simulations in this study are reported in Table 1 . Considering a specific muscular tension of 37 N/cm^2, we calculated a force of 18645 N for the left temporalis muscle and 18780 N for the right one. According to previous assumptions, we estimated that the masseter muscles exerted a force of 1864 N (left) and 1878 N (right). At a gape angle of 20°, the FE simulation generated an anterior bite force of 4312 N, and a posterior bite force of 10103 N. The bite simulation at a greater gape angle (35°) yielded slightly higher values of 4812 N at the anterior end of the dental row and 10823 N at its posterior end.

Table 1. Input muscular data and resulting forces obtained from the biting simulation at 20° and 35° gape angle. Note that all the results have been calculated at a specific tension of 37 N/cm^2.

	Gape angle 20°	Gape angle 35°
Cross-section of the left temporalis muscle	503.93 cm^2	503.93 cm^2
Cross-section of the left masseter muscle	50.39 cm^2	50.39 cm^2
Cross-section of the right temporalis muscle	507.56 cm^2	507.56 cm^2
Cross-section of the right masseter muscle	50.76 cm^2	50.76 cm^2
F temporalis left muscle	18645 N	18645 N
F masseteric left muscle	1864 N	1864 N
F temporalis right muscle	18780 N	18780 N
F masseteric right muscle	1878 N	1878 N
Anterior bite force	**4312 N**	**4812 N**
Posterior bite force	**10103 N**	**10823 N**

We calculated that a posterior bite force of 10823 N would be generated by a great white shark having a body mass of 1542.5 kg and a total length of 536.3 cm. Similarly, an anterior bite force of 4812 N would be generated by a great white shark reaching a body mass of 1249.6 kg and a total length of 501.3 cm.

Based on the FE simulations we also obtained the resulting von Mises stress distributions on the cranium of *Z. varolai* during a biting action (Figure 2). At the two different gape angles (20° and 35°), the stress patterns are almost indistinguishable from each other. The stress values affecting the cranium are between 4 MPa and 19 MPa, with higher values being located in correspondence of the lacrimo-jugal complex and the dental constraints (Figure 2). In the posterior bite simulations (Figure 2a, b, c, d), the stress mainly affects the supracranial basin, with three major peaks being located medial to the left antorbital notch, in correspondence of an anteroposteriorly elongated ridge that is grossly aligned with the right antorbital notch and on the left lateral border of the supracranial basin. The anterior bite load cases exhibit a von Mises stress pattern that is anteriorly projected, involving the rostrum for most of its length (Figure 2e, f, g, h). The von Mises stress values are higher at the base of the rostrum and decrease forward. As we used a cavity-filling 3D mesh, the resulting stress distribution across the supracranial basin could be slightly affected by the lack of modelling of the hollow spaces that are found in this region of the neurocranium (e.g. the facial terminations, the infraorbital canal branches and the nasal cavity). However, this issue should not affect the stress pattern on the rostrum, which appears to be a rather massive structure, lacking apparent foramination.

Discussion

Comparing bite force magnitudes

Much of the biomechanic studies on cetaceans (both extant and extinct) have been focussed on motion, physical properties of tissues, hearing, and sound production; analyses of the feeding mechanics are quite scarce in literature (Fish 1998; de Buffrénil et al. 2000; Rohr and Fish 2004; Yamato et al. 2008; Bagnoli et al. 2011; Loch et al. 2013; Loch and van Vuuren 2016; Tubelli and Ketten 2019). In one of the few investigations about this issue, the bite force of the archaeocete *Basilosaurus isis* was estimated at the specific tension of 37 N/cm^2 (Snively et al. 2015). The posterior and anterior bite forces estimated for *Zygophyseter varolai* at 20° gape angle are, respectively, 39.6% and 66.3% weaker than the

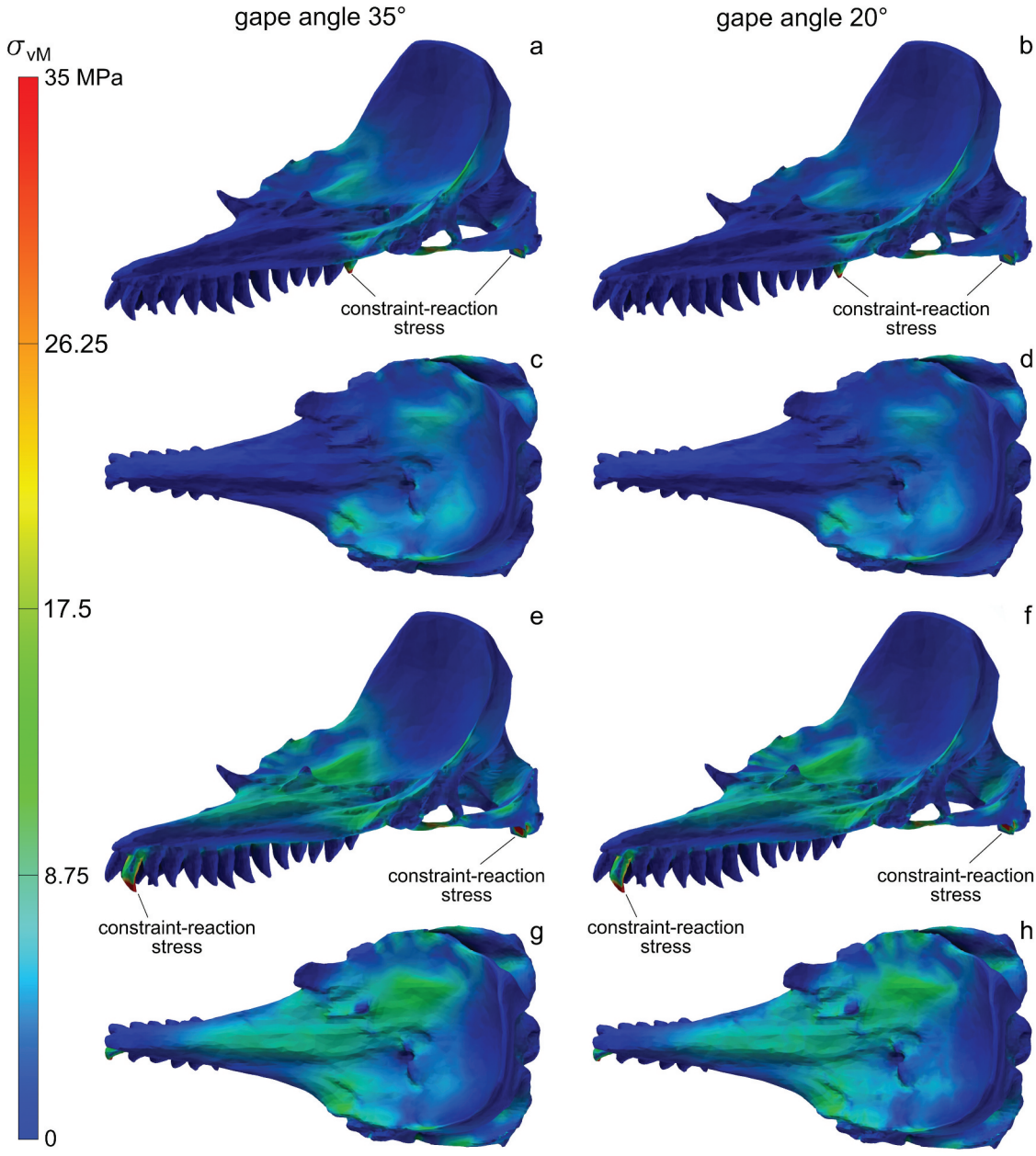

Figure 2. Distribution patterns of the von Mises stress (s_{vM}) on the *Zygophyseter varolai* skull obtained by FEA simulations. a,c) s_{vM} distribution for a posterior bite simulation at 35° gape angle (a, anterolateral view; c, dorsal view). b,d) s_{vM} distribution for a posterior bite simulation at 20° gape angle (b, anterolateral view; d, dorsal view). e,g) s_{vM} distribution for an anterior bite simulation at 35° gape angle (e, anterolateral view; g, dorsal view). f,h) s_{vM} distribution for an anterior bite simulation at 20° gape angle (f, anterolateral view; h, dorsal view).

corresponding values in *B. isis* (Snively et al. 2015). We only compared the *Z. varolai* bite force at 20° because this gape angle is similar to that used for the *B. isis* bite simulations (measured from Snively et al. 2015: Figure 1a). The disparity of bite force values between *Z. varolai* and *B. isis* is not surprising: indeed, *Z. varolai* displays a smaller cross-section of the temporalis muscle, and consequently, a less developed mandible adduction power. Furthermore, *Z. varolai* bears a proportionally more elongated rostrum than *B. isis*; this is clear when comparing the ratios between the length of the rostrum and the distance between the tip of the rostrum and the posteriormost point of the temporal fossa in *Z. varolai* (0.56) and *B. isis* (0.51). This morphological difference may contribute to the large gap between the anterior bite force of *Z. varolai* and that of *B. isis*.

We calculated the hypothetical body length (501.3–536.3 cm) and mass (1249.6–1542.5 kg) of a great white shark (*Carcharodon carcharias*) that would exert the same bite force as estimated for *Z. varolai* at a gape angle of 35°. We noted a slight discrepancy between the datum calculated for the anterior and posterior bite forces; this can be easily explained by considering that the force dispersion is greater along the elongated rostrum of *Z. varolai* than along the short and rounded mouth arch of *C. carcharias*. Regardless for this, our results suggest that *Z. varolai* generated the same bite force as a fully adult great white shark (Long and Jones 1996; Estrada et al. 2006).

We also compared the biting performances of *Z. varolai* with those of the extant saltwater crocodile (*Crocodylus porosus*, the largest living reptile) at the caniniform and molariform teeth (Read et al. 2007). Saltwater crocodiles grow throughout their life

span, and consequently, their bite force greatly increases with age (Erickson et al. 2012). The highest bite force recorded by Erickson et al. (2012) for a saltwater crocodile is 11216 N (at the caniniform tooth) and 16414 N (at the molariform tooth) in a 459 cm long individual with a skull length of 65 cm; these results are higher than the bite forces estimated for *Z. varolai* and place *C. porosus* near to *B. isis* (Erickson et al. 2012). This is even more surprising considering that *Z. varolai* exhibits a body that is about 1.5 times longer and a cranium that is more than twice as long than the tested individual of *C. porosus* (Bianucci and Landini 2006; Erickson et al. 2012). The reason behind these exceptional values in *C. porosus* could be searched in the reptilian cranial and muscular architecture. Indeed, reptiles have laterally unconstrained pterygoid muscles and highly pennate temporalis muscles that exert a higher specific tension than mammals. Thus, the lack of bony restrictions, and the resulting greater space available for the muscle expansion in reptiles might explain the high bite force values observed in *C. porosus* (Thomason 1991; Christiansen 2007; Erickson et al. 2012; Snively et al. 2015).

According to an estimation made via the 'dry-skull' method and adjusted for the pennation of the mammalian musculature, the lion (*Panthera leo*) can exert a bite force of 3388 N at the canine (McHenry et al. 2007). The lion is one of the largest extant felids and is known to use a powerful bite to hold and kill its prey (Sunquist and Sunquist 2002; McHenry et al. 2007; Schaller 2009). In felids, the canine tooth is placed in an anterior position along the tooth row, thus we compared the canine bite force of *P. leo* with the anterior bite force estimated for *Z. varolai*. Despite the long rostrum, and thus the relative force dispersion, *Z. varolai* results in having a 21.4–29.6% higher anterior bite force value than the canine bite force of *P. leo* (McHenry et al. 2007).

According to our simulation, in condition of static bite, *Z. varolai* can generate a force of more than 10000 N at the posteriormost tooth, depending on the gape angle. It has been calculated that 7000–9000 N are needed to break a long bone of a large ungulate (Tanner et al. 2008). In addition, Erickson et al. (1996) estimated that the giant theropod dinosaur *Tyrannosaurus rex* had to generate at least 6410 N to damage a *Triceratops* ilium. Based on these lines of evidence, *Z. varolai* was likely able to break or seriously damage the bones of a prey by using its powerful posterior bite. Given all these considerations, we hypothesise that *Z. varolai* was able to generate a great bite force, even compared with other marine and terrestrial vertebrate predators known to use biting actions for capturing, killing, and sometimes processing (i.e., cutting or tearing) their prey items.

Feeding strategy by biomechanics

The high bite force values associated to *Zygophyseter varolai* are in good agreement with several osteomorphological and dental characters of this extinct sperm whale, including a wide temporal fossa, a well-developed zygomatic process of the squamosal, and the presence of deep occlusal facets on teeth suggesting a strong degree of occlusion during bite (Bianucci and Landini 2006).

The mouth gape angle and the point where the reaction force is measured are two important factors in a FE bite simulation (Bourke et al. 2008; Wroe et al. 2008). Our results reveal that the bite force estimated at 35° gape angle is higher than that at 20° gape angle (both anteriorly and posteriorly); probably, 35° is close to the angle at which the highest bite force is generated (i.e., the optimum of the mechanical advantage) (Bourke et al. 2008; Wroe et al. 2008). Future research efforts might investigate the variation of bite force values with the gape angle increase, which is especially relevant in the light of the wide mouth opening hypothesised for *Z. varolai* (Bianucci and Landini 2006).

In our simulations, we recorded a higher bite force at the posterior most dental constraint relative to the anteriorly positioned constraint. This trend is not unexpected, because the posteriormost tooth is closer to the rotation centre of the mandible (mandibular fossa), and as such, to the lever fulcrum. Consequently, the huge disparity between the anterior and posterior bite forces is a direct consequence of the mandible lever mechanics (Wroe et al. 2008; Lambert et al. 2014). Interestingly, bony outgrowths that have been detected along the upper dental row in MUSM 1399, the holotype of *Acrophyseter robustus* (a macroraptorial sperm whale phylogenetically and morphologically close to *Z. varolai*; Lambert et al. 2014, 2017), are especially developed nearby the posteriormost teeth. These bony outgrowths have been interpreted as resulting from the occlusal stress increase close to the rotation centre of the mandible lever system (Lambert et al. 2014). Thus, the bony exostoses observed in *A. robustus* and their functional interpretation further support the bite force trend described by our bite simulations in *Z. varolai*. Such a variation of bite force along the upper jaw provides some clues about the feeding strategy of *Z. varolai*: this macroraptorial sperm whale likely captured large food items with an anterior bite and then cut them into pieces with a powerful posterior bite. The anteriorly tapered rostrum and the procumbent conical anterior teeth could have been used to efficiently grab motile preys (Bianucci and Landini 2006). On the other hand, the posterior mandibular teeth (the sole that were found within the corresponding alveoli) display an obvious degree of mediolateral compression of the root portion placed above the gingival collar that possibly facilitated the shearing of food items (Bianucci and Landini 2006). Even though this character could simply reflect the accommodation of the voluminous lower cheek teeth within the narrow space left by the large mandibular canal running through the posterior portion of the dentary, the mediolateral compression of the posterior postcanines might still represent an exaptation facilitating the shearing of prey items.

Many morphological features among those listed above (e.g., the anteriorly tapered rostrum, the wide temporal fossa, the procumbent anterior teeth) are shared between *Z. varolai* and *Acrophyseter* spp.; in addition, both *Z. varolai* and *A. deinodon* display a mediolateral compression of the posterior mandibular teeth (Bianucci and Landini 2006; Lambert et al. 2008, 2017). Based on these shared morphological characters, we propose for *Zygophyseter* and *Acrophyseter* a 'grip-and-shear' feeding strategy consisting of three phases: 1) grasping and piercing of the prey with the anterior teeth, 2) moving the food item backward along the mouth, and 3) cutting it with the posterior teeth. In Figure 3, this hypothetical trophic behaviour is integrated within the framework of feeding strategies proposed for extant marine mammals by Kienle et al. (2017) and Berta and Lanzetti (2020). It is our content that such a feeding strategy was also used by heterodont basilosaurids having anterior conical teeth (canine and incisors) and even more mediolaterally compressed posterior teeth (premolars and molars) (Uhen 2004; Fahlke 2012; Fahlke et al. 2013; Loch et al. 2015; Snively et al. 2015) and, as a plesiomorphic condition, by several heterodont basal neocetes (e.g., squalodontids; see Loch et al. 2015; Collareta et al. 2020a). Nevertheless, the trophic strategy of *Zygophyseter* and *Acrophyseter* can hardly be considered as plesiomorphic. Indeed, neither *Eudelphis motzelensis* nor the recently described *Raphicetus valenciae*, both of which appear to have branched earlier than *Acrophyseter* spp. and *Z. varolai*, display any osteological or dental feature that could be positively associated with a macropredator ecology (Lambert 2008; Lambert et al. 2020). Considering also the incipient homodonty observed in all physeteroids (in which all teeth feature one root and no accessory cusps), we interpret the feeding strategy of *Zygophyseter* and *Acrophyseter* as a secondary re-

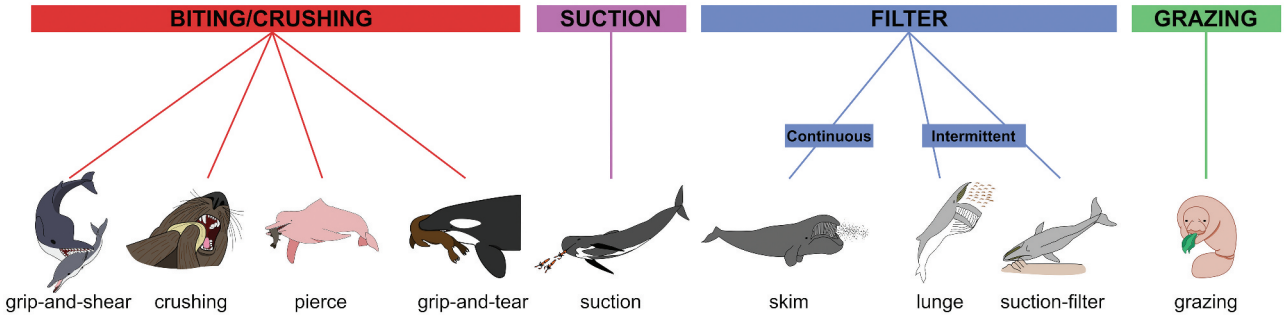

Figure 3. Feeding strategies of marine mammal predators. Modified from Berta and Lanzetti (2020), with the addition of the grip-and-shear feeding (illustration of *Zygophyseter varolai* modified from Bianucci and Landini 2006).

adaptation driven by a selective pressure towards a diet consisting of large-bodied prey. A tooth morphology roughly similar to that of *Z. varolai* and *Acrophyseter* spp. is also observed in some fossil homodont odontocetes, e.g. the early Miocene *Furcacetus flexirostrum,* which is characterised by large and procumbent upper incisors (Bianucci et al. 2020). However, based on the delicate sigmoidal rostrum and the moderately expanded temporal fossa, *F. flexirostrum* is believed to have used the anterolaterally oriented teeth to catch quickly moving prey items such as shrimps and small fishes (Bianucci et al. 2020). Similarly, the living river dolphin *Platanista gangetica* uses the large and pointed (but not procumbent) anterior teeth and slender rostrum to grab and pierce small preys, the latter being subsequently moved towards the throat without being sheared (Pilleri 1970; McCurry et al. 2017).

The grip-and-shear feeding technique is not observed among extant sarcophagous predators, since they hold and shake their prey with the jaws to tear off large pieces of flesh (Figure 3), without a proper cutting action (Werth 2000; Berta and Lanzetti 2020). This shark-like feeding strategy is known as grip-and-tear (Figure 3), and the sole extant cetaceans that use it are the killer whale (*Orcinus orca*) and the false killer whale (*Pseudorca crassidens*) (Ford 2018; Berta and Lanzetti 2020; Galatius et al. 2020). These large-sized delphinids have a blunt and robust rostrum as well as cheek teeth that are not laterally compressed (Werth 2006a; McCurry et al. 2017; Ford 2018; Berta and Lanzetti 2020; Galatius et al. 2020), thus differing from the putative grip-and-shear feeders like *Z. varolai* and *B. isis* (Uhen 1996; Bianucci and Landini 2006). Regardless of the differences between the aforementioned trophic strategies, the teeth of *O. orca* display long occlusion facets (pers. obs. on MSNUP C298 and MSNUP C301) that are reminiscent of the condition observed in *Z. varolai* and *Acrophyseter* spp. (Bianucci and Landini 2006; Lambert et al. 2008, 2014, 2017). However, the presence of well-developed occlusal facets is only indicative of a strong dental occlusion and an extensive use of the biting action during feeding (Bianucci and Landini 2006; Lambert et al. 2017; Lambert and Bianucci 2019; Peri et al. 2020). Furthermore, during a grip-and-tear feeding event, the predator tears its prey into pieces with large bites, thus exerting a somewhat ripping action (Werth 2006a; Berta and Lanzetti 2020). According to our hypothesis, a grip-and-shear feeder would rather use a posterior bite to cut its prey after capturing it with an anterior bite. Therefore, the fundamental difference between these two feeding strategies relies on how the biting action is used for prey processing.

Thus, during the first phase of a grip-and-shear feeding action, the prey is grabbed with an anterior bite; during the second phase, it is moved posteriorly along the mouth towards the posterior tooth rows; finally, during the third phase, it is sheared with a powerful posterior bite. In our simulations of the anterior bite of *Z. varolai* (Figure 2e, f, g, h), the stress pattern appears as projected towards the tip of the rostrum, and the higher values are placed at the rostrum base. This is a consequence of the mechanical response of an elongated body being subjected to a force application at one of its ends. In these conditions, the base of an elongated rostrum is a 'bending point' where the tensile stress accumulates. Consequently, the von Mises stress pattern resulting from our FE model replicates well the first phase of a grip-and-shear feeding action. After capture, the wounded prey was likely transported towards the posterior portion of the mouth, possibly by means of suction. Interestingly, the living sperm whale *P. macrocephalus* can create a powerful suction at level of the gular cavity (Werth 2006a), thus evoking the possibility that extinct physeteroids were also capable of applying some degree of suction. Moreover, a phase of transport of the food items by means of suction is observed in extant raptorial longirostrine odontocetes (e.g., *Inia geoffrensis*) as well as in the more stoutly snouted *Tursiops* (Werth 2000, 2006a, 2006b; Bloodworth and Marshall 2005). In the posterior bite simulations, the rostrum does not appear as stressed, except for its very basal portion, close to the constraint at the posteriormost tooth (Figure 2a, b, c, d). Here, the FEA shows an evident stress peak that is probably related to the contact between the tooth and the food item during the third phase of a grip-and-shear feeding action. Based on these observations, the stress patterns resulting from our FEA simulations appear as consistent with the feeding strategy hypothesised above for *Z. varolai*. Interestingly, there is a peak of stress insisting on the right side of the supracranial basin, in correspondence of an evident ridge. This structure might counteract the bending of the rostrum during a biting action, and especially in occasion of an anterior bite (Figure 2). However, as already mentioned, the lack of modelling of the internal cranial geometry of the cranium of *Z. varolai* prevents us from further anatomical and functional interpretations of specific stress peaks while allowing for a more general discussion of stress distribution on the neurocranium and, especially, the rostrum.

Palaeoecological role and diet of Zygophyseter varolai

According to our estimates, *Zygophyseter varolai* was able to generate the same bite force as a great white shark individual well beyond sexual maturity (Kohler et al. 1996; Wroe et al. 2008). Extant *Carcharodon carcharias* is known as a highly generalist predator that mainly feeds upon diminutive and fat-rich marine mammals, such as fur seals and small toothed whales (Compagno 1984; Heithaus 2001; Brown et al. 2010; Skomal et al. 2017; Moro et al. 2020). Several field studies and laboratory analyses have demonstrated that extant white sharks prey upon marine mammals

in adulthood, when they reach a body length of 300–400 cm (Long and Jones 1996; Estrada et al. 2006). Considering that the body length of the holotype of *Z. varolai* was likely 650–700 cm (Bianucci and Landini 2006), its ecology might have been somewhat similar to that of an adult *C. carcharias*, and its diet mainly consisting of medium-sized marine vertebrates. As already mentioned, *Z. varolai* was retrieved from the Tortonian strata of the Cisterna quarry (Lecce), which also provided remains of several other marine vertebrates, such as *Messapicetus longirostris* (Ziphiidae, Cetacea), *Metaxytherium medium* (Dugongidae, Sirenia), *Makaira* cf. *M. nigricans* (Istiophoriade, Perciformes) and *Acanthocibius* cf. *A. solandri* (Scombridae, Perciformes) (Bianucci et al. 1992, 2003, 2016a; Carnevale et al. 2002); all of them would have been potential prey items for *Z. varolai*. Besides *Z. varolai*, the Tortonian strata of the Pietra leccese formation have yielded fossils of other marine macropredators, including an unnamed macroraptorial sperm whale found at approximately the same horizon as the holotype of *Z. varolai* (Peri et al. 2020) and several large-sized sharks (e.g., *Anotodus agassizi, Carcharocles megalodon, Cosmopolitodus hastalis, Parotodus benedeni*) (Menesini 1969). Such an abundance of high trophic-level predators in the Mediterranean Basin during the early late Miocene starkly contrasts with the present-day situation, which sees the great white shark and occasionally the killer whale as the sole apex predators to be found in the Mediterranean trophic chains (Notarbartolo di Sciara et al. 1993; Morey et al. 2003; Abdulla 2004; Notarbartolo di Sciara and Reeves 2006; Notarbartolo di Sciara 2016). The late Miocene presence of multiple top predators has previously been explained with high productivity conditions that led to a high availability of food items for a broad spectrum of marine vertebrates (Peri et al. 2020). Sedimentologic evidence of high productivity, such as phosphate-rich levels associated with glauconite, has been reported from several localities of the central Mediterranean (Salento Peninsula, Sicily, Malta and Crete) (Föllmi et al. 2008, 2015; Catanzariti and Gatt 2014; Vescogni et al. 2018). This suggests the presence of nutrient-laden currents from the eastern Mediterranean that replenished the central basin and supported the late Miocene macropredator guild retrieved from the Pietra leccese formation (Menesini 1969; Bianucci and Landini 2006; Peri et al. 2020).

Remarks on the Miocene marine macropredators

The results obtained in this study need to be framed in the context of the complex ecology of Miocene seas. Indeed, besides a number of genera and species that are based on taxonomically diagnostic skeletal materials, isolated teeth referable to macroraptorial physeteroids have been reported from middle and upper Miocene deposits of several localities of the Americas, Asia and Europe (e.g., Kimura et al. 2006; Hasegawa et al. 2006; Marra et al. 2016; Reumer et al. 2017; Piazza et al. 2018; Lambert and Bianucci 2019). As already mentioned, the chronostratigraphic and geographic distribution of the published remains of macroraptorial sperm whales suggests that this group impressively radiated during the middle and late Miocene (Lambert et al. 2017). In the light of the presence of at least six species of macropredator sperm whales (*Acrophyseter deinodon, A. robustus, Livyatan melvillei, Zygophyseter varolai*, and two unnamed taxa identified from isolated dental remains by Marra et al. 2016 and Peri et al. 2020) during the late Miocene, the present-day stock of high-trophic level odontocete predators appears greatly depleted, with two delphinids – i.e., the killer whale (*Orcinus orca*) and the false killer whale (*Pseudorca crassidens*) – being the sole macropredators among living toothed whales (Baird et al. 2008; Barrett-Lennard et al. 2011; Ford et al. 2011; Pitman et al. 2015; Ford 2018; Baird 2018; Galatius et al. 2020). Considering the taxonomic composition of the highest trophic levels, a shift likely occurred in Plio-Pleistocene epochs, with sperm whales (acting as apex consumers in the late Miocene) being replaced in this trophic position by large-sized delphinids. Besides macroraptorial sperm whales, large-sized elasmobranchs like *Anotodus agassizii, Carcharocles megalodon, Cosmopolitodus hastalis* and *C. plicatilis* roamed the seas as apex predators during the middle and late Miocene (Menesini 1969; Purdy et al. 2001; Collareta et al. 2017a, 2017b; Boessenecker et al. 2019; Landini et al. 2017; Perez et al. 2018). On the other hand, large-sized extant lamnid and carcharhinid sharks (e.g., *Carcharhinus leucas, Carcharodon carcharias* and *Galeocerdo cuvier*) are often regarded as top predators within their habitats (Long and Jones 1996; Simpfendorfer et al. 2001; Estrada et al. 2006; Kim et al. 2012; Heupel et al. 2014); however, they do not reach the giant size of mega-toothed sharks of the Miocene (Collareta et al. 2017a; Boessenecker et al. 2019).

All things considered, the late Miocene oceans displayed a greater diversity of large-sized macropredators than today; in addition, several such forms have been retrieved in the same sedimentary bodies, thus suggesting a cohabitation in the same marine areas (e.g. Carnevale et al. 2002; Bianucci et al. 2016; Peri et al. 2020; Bosio et al. 2021). Nowadays, macroraptorial sperm whales are extinct, and the reasons behind this disappearance are tentatively traced back to the late Neogene establishment of gigantism as the size standard among baleen whales (Lambert et al. 2010; Marx and Fordyce 2015; Slater et al. 2017; Bianucci et al. 2019). Furthermore, a global cooling occurred at the end of the Miocene (about 7–5.4 Ma) may have reduced the geographical range of these macroraptorial physeteroids and led to the disappearance of medium-sized baleen whale faunas (Lambert et al. 2010; Herbert et al. 2016; Tanner et al. 2020). Similar biotic and abiotic drivers, together with the emergence of modern ecomorphotypes such as those represented by the great white shark and the killer whale, have been evoked for explaining the decline and the extinction of the otodontid lineage in the early Pliocene (ca. 5.3–3.5 Ma) (Collareta et al. 2017a; Boessenecker et al. 2019; Pimiento et al. 2019).

Conclusions and perspectives

We used the 'dry skull' method and the finite element analysis (FEA) to estimate the bite force of the macroraptorial sperm whale *Zygophyseter varolai* from the late Miocene of southern Italy. We set four different load cases to obtain anterior and posterior bite force estimated at 20° and 35° gape angles. From the FEA simulation, we obtained an estimation of 4312 N (20° gape angle) and 4812 N (35° gape angle) for the anterior bite. We also estimated that *Z. varolai* generated 10103 N (20° gape angle) and 10823 N (35° gape angle) at the posterior bite.

Through mathematical formulas, we calculated that *Z. varolai* exerted the same bite force of an adult great white shark reaching more than 500 cm of body length. Extant white sharks begin to prey upon marine mammals when they reach 300–400 cm of body length. Consequently, we hypothesise that *Z. varolai* had an analogous diet and that it fed upon the small and medium-sized marine vertebrate fauna retrieved from the Tortonian strata of the Pietra leccese formation.

The obtained bite force results are similar to, though somewhat lower than, those estimated in the basilosaurid archaeocete *Basilosaurus isis* in a previous study. According to our estimations, *Z. varolai* exerted a high bite force, most likely sufficient to break the bones of its prey. Based on the bite force variations along the maxilla and the teeth and cranial morphology of Z. *varolai*, we hypothesise that this extinct sperm whale grasped its food item

with an anterior bite, moved it backward along the mouth and finally cut it with a powerful posterior bite. This hypothetic feeding strategy, here named 'grip-and-shear', was likely shared by the phylogenetically and morphologically close sperm whale genus *Acrophyseter*. Some modern odontocetes use slightly different feeding strategies as they grab and tear apart large-sized food items (grip-and-tear feeding), snap small preys with anterior pointed teeth to swallow them entirely (pierce feeding) or smash them with their posterior teeth (crushing feeding). The stress patterns derived from the FEA appear as consistent with the grip-and-shear feeding strategy proposed for *Z. varolai*: the anterior bite simulations show a stress pattern that is anteriorly projected on the rostrum, while the posterior bite simulations reveal a stress peak at the rostrum base that replicates the contact between the posterior cutting tooth and the food item.

This is the first study that investigates the bite mechanics of a macroraptorial physeteroid using FEA. Such a biomechanical approach might be applied to shed new light on the trophic spectrum and the feeding strategies of other macroraptorial sperm whales, including the giant putative whale-eater *Livyatan melvillei*. A better understanding of these aspects will greatly contribute to unravel the complex trophic relationships in the Miocene oceans, which were home to a surprisingly high diversity of large-sized predators.

Acknowledgments

We are grateful to Chiara Sorbini for providing access to the palaeontological material studied in the present work. We also thank Olivier Lambert and Toshiyuki Kimura who greatly contributed to improve the quality of this paper with their useful advice. Not least, we are grateful to Gareth Dyke for his expert editorial support.

Disclosure statement

No potential conflict of interest was reported by the author(s).

ORCID

Emanuele Peri http://orcid.org/0000-0001-8635-5379
Peter L. Falkingham http://orcid.org/0000-0003-1856-8377
Alberto Collareta http://orcid.org/0000-0002-6513-8882
Giovanni Bianucci http://orcid.org/0000-0001-7105-0863

References

Abdulla A. 2004. Status and conservation of sharks in the Mediterranean Sea. IUCN Tech Pap. 144:1–6.

Alam P, Amini S, Tadayon M, Miserez A, Chinsamy A. 2016. Properties and Architecture of the Sperm Whale Skull Amphitheatre. Zoology. 119(1):42–51. https://doi.org/10.1016/j.zool.2015.12.001

Anderson PSL, Westneat MW. 2009. A biomechanical model of feeding kinematics for *Dunkleosteus terrelli* (Arthrodira, Placodermi). Paleobiology. 35 (2):251–269. doi:10.1666/08011.1.

Bagnoli P, Cozzi B, Zaffora A, Acocella F, Fumero R, Laura Costantino M. 2011. Experimental and computational biomechanical characterisation of the tracheo-bronchial tree of the bottlenose dolphin (*Tursiops truncatus*) during diving. J Biomech. 44(6):1040–1045.

Baird RW. 2018. False Killer Whale: *pseudorca crassidens*. In: Würsig B, Jgm T, Km K, editors. Encyclopedia of Marine Mammals. Third Edition ed. San Diego (CA): Academic Press; p. 347–349.

Baird RW, Gorgone AM, McSweeney DJ, Webster DL, Salden DR, Deakos MH, Ligon AD, Schorr GS, Barlow J, Mahaffy SD. 2008. False killer whales (*Pseudorca crassidens*) around the main Hawaiian Islands: long-term site fidelity, inter-island movements, and association patterns. Mar Mammal Sci. 24(3):591–612.

Barrett-Lennard LG, Matkin CO, Durban JW, Saulitis EL, Ellifrit D. 2011. Predation on gray whales and prolonged feeding on submerged carcasses by transient killer whales at Unimak Island, Alaska. Mar Ecol Prog Ser. 421:229–241.

Bates KT, Falkingham PL. 2018. The importance of muscle architecture in biomechanical reconstructions of extinct animals: a case study using *Tyrannosaurus rex*. J Anat. 233(5):625–635.

Bell PR, Snively E, Shychoski L. 2009. A comparison of the jaw mechanics in hadrosaurid and ceratopsid dinosaurs using finite element analysis. Anat Rec. 292(9):1338–1351.

Berta A, Lanzetti A. 2020. Feeding in marine mammals: an integration of evolution and ecology through time. Palaeontol Electron. 23(2):1–42.

Bianucci G, Collareta A, Post K, Varola A, Lambert O. 2016a. A new record of *Messapicetus* from the Pietra Leccese (late Miocene, Southern Italy): anti-tropical distribution in a fossil beaked whale (Cetacea, Ziphiidae). Riv Ital Paleontol S. 122(1):63–74.

Bianucci G, De Muizon C, Urbina M, Lambert O. 2020. Extensive diversity and disparity of the early Miocene platanistoids (Cetacea, odontoceti) in the Southeastern Pacific (Chilcatay Formation, Peru). Life. 10. doi:10.3390/life10030027.

Bianucci G, Di Celma C, Landini W, Post K, Tinelli C, De Muizon C, Gariboldi K, Malinverno E, Cantalamessa G, Gioncada A, et al. 2016. Distribution of fossil marine vertebrates in Cerro Colorado, the type locality of the giant raptorial sperm whale *Livyatan melvillei* (Miocene, Pisco Formation, Peru). J Maps. 12(3):543–557.

Bianucci G, Landini W. 2006. Killer sperm whale: a new basal physeteroid (Mammalia, Cetacea) from the Late Miocene of Italy. Zool J Linn Soc-Lond. 148(1):103–131.

Bianucci G, Landini W, Varola A. 1992. *Messapicetus longirostris*, a new genus and species of Ziphiidae (Cetacea) from the late Miocene of 'Pietra leccese' (Apulia, Italy). Boll Soc Paleontol I. 31(2):261–264.

Bianucci G, Landini W, Varola A. 2003. New records of *Metaxytherium* (Mammalia: Sirenia) from the late Miocene of Cisterna quarry (Apulia, southern Italy). Boll Soc Paleontol I. 42(1–2):59–63.

Bianucci G, Marx FG, Collareta A, Di Stefano A, Landini W, Morigi C, Varola A. 2019. Rise of the titans: baleen whales became giants earlier than thought. Biol Letters. 15:5. doi:10.1098/rsbl.2019.0175

Bianucci G, Varola A. 2014. I cetacei fossili della Pietra leccese nei musei del Salento [Fossil cetaceans from the Pietra leccese formation in the Salento museums]. Museol Sci Mem. 13:130–134.

Bloodworth B, Marshall CD. 2005. Feeding kinematics of *Kogia* and *Tursiops* (Odontoceti: cetacea): characterization of suction and ram feeding. J Exp Biol. 208(19):3721–3730.

Boersma AT, Pyenson ND. 2015. *Albicetus oxymycterus*, a new generic name and redescription of a basal physeteroid (Mammalia, Cetacea) from the Miocene of California, and the evolution of body size in sperm whales. PLoS One. 10 (12):e0135551.

Boessenecker RW, Churchill M, Buchholtz EA, Beatty BL, Geisler JH. 2020. Convergent Evolution of Swimming Adaptations in Modern Whales Revealed by a Large Macrophagous Dolphin from the Oligocene of South Carolina. Curr Biol. 30(16):3267–3273.e2.

Boessenecker RW, Ehret DJ, Long DJ, Churchill M, Martin E, Boessenecker SJ. 2019. The early Pliocene extinction of the mega-toothed shark *Otodus megalodon*: a view from the eastern North Pacific. PeerJ. 7(2):e6088.

Bosio G, Collareta A, Di Celma C, Lambert O, Marx FG, De Muizon C, Gioncada A, Gariboldi K, Malinverno E, Varas-Malca R, et al. 2021. Taphonomy of marine vertebrates of the Pisco Formation (Miocene, Peru): insights into the origin of an outstanding Fossil-Lagerstätte. PLoS One. 16 (17):e0254395. doi:10.1371/journal.pone.0254395.

Bourke J, Wroe S, Moreno K, McHenry C, Clausen P. 2008. Effects of gape and tooth position on bite force and skull stress in the dingo (*Canis lupus dingo*) using a 3-dimensional finite element approach. PLoS One. 3(5):e2200. doi:10.1371/journal.pone.0002200.

Brown AC, Lee DE, Bradley RW, Anderson S. 2010. Dynamics of white shark predation on pinnipeds in California: effects of prey abundance. Copeia. 2010 (2):232–238.

Bullard TS, Caldwell MW. 2010. Redescription and rediagnosis of the tylosaurine mosasaur *Hainosaurus pembinensis* Nicholls, 1988, as *Tylosaurus pembinensis* (Nicholls, 1988). J Vertebr Paleontol. 30(2):416–426.

Carnevale G, Sorbini C, Landini W, Varola A. 2002. *Makaira* cf. *M. nigricans* Lacepede, 1802 (Teleostei: Perciformes: istiophoridae) from the Pietra Leccese, Late Miocene, Apulia, Southern Italy. Palaeontogr Ital. 88:63–75.

Catanzariti R, Gatt M. 2014. Calcareous nannofossil biostratigraphy from the middle/late Miocene of Malta and Gozo (Central Mediterranean). Stratigraphy. 11(18):303–336.

Christiansen P. 2007. Comparative bite forces and canine bending strength in feline and sabretooth felids: implications for predatory ecology. Zool J Linn Soc-Lond. 151(2):423–437.

Collareta A, Di Cencio A, Ricci R, Bianucci G. 2020a. The shark-toothed dolphin *Squalodon* (Cetacea: odontoceti) from the remarkable montagna della Majella marine vertebrate assemblage (Bolognano formation, Central Italy).

Carnets Geol. 20(2):19–28.
Collareta A, Lambert O, De Muizon C, Palomino AMB, Urbina M, Bianucci G. 2020b. A new physeteroid from the late Miocene of Peru expands the diversity of extinct dwarf and pygmy sperm whales (Cetacea: odontoceti: kogiidae). C R Palevol. 95(5):79–100.
Collareta A, Lambert O, Landini W, Di Celma C, Malinverno E, Varas-Malca R, Urbina M, Bianucci G. 2017a. Did the giant extinct shark *Carcharocles megalodon* target small prey? Bite marks on marine mammal remains from the late Miocene of Peru. Palaeogeogr Palaeocl. 469:84–91.
Collareta A, Landini W, Chacaltana C, Valdivia W, Altamirano-Sierra A, Urbina-Schmitt M, Bianucci G. 2017b. A well preserved skeleton of the fossil shark *Cosmopolitodus hastalis* from the late Miocene of Peru, featuring fish remains as fossilized stomach contents. Riv Ital Paleontol S. 123(1):11–22. doi:10.13130/2039-4942/8005.
Compagno LJV 1984. FAO species catalogue. Vol. 4. Sharks of the world. An annotated and illustrated catalogue of shark species known to date. Part 2. Carcharhiniformes FAO Fish Synopsis. 251–655.
Cooper JA, Pimiento C, Ferrón HG, Benton MJ. 2020. Body dimensions of the extinct giant shark *Otodus megalodon*: a 2D reconstruction. Sci Rep. 10:14596. doi:10.1038/s41598-020-71387-y
de Buffrénil V, Sire J-Y SD. 1986. Comparaison de la structure et du volume squelettiques entre un delphinidé (*Delphinus delphis* L.) et un mammifère terrestre (*Panthera leo* L.) [Comparison of skeletal structure and volume between a delphinid (*Delphinus delphis* L.) and a land mammal (*Panthera leo* L.)]. Can J Zool. 64(8):1750–1756.
de Buffrénil V, Zylberberg L, Traub W, Casinos A. 2000. Structural and mechanical characteristics of the hyperdense bone of the rostrum of *Mesoplodon densirostris* (Cetacea, Ziphiidae): summary of recent observations. Hist Biol. 14(1–2):57–65.
Díez Díaz V, Mallison H, Asbach P, Schwarz D, Blanco A. 2021. Comparing surface digitization techniques in palaeontology using visual perceptual metrics and distance computations between 3D meshes. Palaeontology. 64 (2):179–202.
Driscoll DA, Dunhill AM, Stubbs TL, Benton MJ. 2019. The mosasaur fossil record through the lens of fossil completeness. Palaeontology. 62(1):51–75.
Ehret DJ, Ebersole J. 2014. Occurrence of the megatoothed sharks (Lamniformes: otodontidae) in Alabama, USA. PeerJ. 2(1):1–18.
Erickson GM, Gignac PM, Steppan SJ, Lappin AK, Vliet KA, Brueggen JD, Inouye BD, Kledzik D, Webb GJW. 2012. Insights into the ecology and evolutionary success of crocodilians revealed through bite-force and tooth-pressure experimentation. PLoS One. 7(3):e31781. doi:10.1371/journal.pone.0254395.
Erickson GM, Van Kirk SD, Su J, Levenston ME, Caler WE, Carter DR. 1996. Bite-force estimation for *Tyrannosaurus rex* from tooth-marked bones. Nature. 382(6593):706–708.
Estrada JA, Rice AN, Natanson LJ, Skomal GB. 2006. Use of isotopic analysis of vertebrae in reconstructing ontogenetic feeding ecology in white sharks. Ecology. 87(4):829–834.
Fahlke JM. 2012. Bite marks revisited – evidence for middle-to-late Eocene *Basilosaurus isis* predation on *Dorudon atrox* (both Cetacea, Basilosauridae). Palaeontol Electron. 15(3):32A. doi:10.26879/341.
Fahlke JM, Autenrieth M. 2016. Photogrammetry vs. Micro-CT scanning for 3D surface generation of a typical vertebrate fossil - a case of study. J Paleontol Tech. 14:1–18.
Fahlke JM, Bastl KA, Semprebon GM, Gingerich PD. 2013. Paleoecology of archaeocete whales throughout the Eocene: dietary adaptations revealed by microwear analysis. Palaeogeogr Palaeocl. 386:690–701.
Falkingham PL. 2012. Acquisition of high resolution three-dimensional models using free, open-source, photogrammetric software. Palaeontol Electron. 15 (1):1T. doi:10.26879/264.
Falkingham PL, Bates KT, Avanzini M, Bennett M, Bordy EM, Breithaupt BH, Castanera D, Citton P, Díaz-Martínez I, Farlow JO, et al. 2018. A standard protocol for documenting modern and fossil ichnological data. Palaeontology. 61(4):469–480.
Falkingham PL, Bates KT, Farlow JO. 2014. Historical photogrammetry: bird's Paluxy River dinosaur chase sequence digitally reconstructed as it was prior to excavation 70 years ago. PLoS One. 9(4):e93247. doi:10.1371/journal.pone.0093247.
Falkingham PL, Turner ML, Gatesy SM. 2020. Constructing and testing hypotheses of dinosaur foot motions from fossil tracks using digitization and simulation. Palaeontology. 63(6):865–880.
Fau M, Cornette R, Houssaye A. 2016. Photogrammetry for 3D digitizing bones of mounted skeletons: potential and limits. C R Palevol. 15(8):968–977.
Ferrón HG, Martínez-Pérez C, Botella H. 2017. Ecomorphological inferences in early vertebrates: reconstructing *Dunkleosteus terrelli* (Arthrodira, Placodermi) caudal fin from palaeoecological data. PeerJ. 5(12):1–20.
Fish FE. 1998. Comparative kinematics and hydrodynamics of odontocete cetaceans: morphological and ecological correlates with swimming performance. J Exp Biol. 201(20):2867–2877.
Foffa D, Cuff AR, Sassoon J, Rayfield EJ, Mavrogordato MN, Benton MJ. 2014. Functional anatomy and feeding biomechanics of a giant Upper Jurassic pliosaur (Reptilia: sauropterygia) from Weymouth Bay, Dorset, UK. J Anat. 225(2):209–219.
Föllmi KB, Gertsch B, Renevey J-P, De Kaenel E, Stille P. 2008. Stratigraphy and sedimentology of phosphate-rich sediments in Malta and south-eastern Sicily (latest Oligocene to early Late Miocene). Sedimentology. 55(4):1029–1051.
Föllmi KB, Hofmann H, Chiaradia M, De Kaenel E, Frijia G, Parente M. 2015. Miocene phosphate-rich sediments in Salento (southern Italy). Sediment Geol. 327:55–71.
Ford JKB. 2018. Killer Whale: *orcinus orca*. In: Würsig B, Jgm T, Km K, editors. Encyclopedia of Marine Mammals. Third Edition ed. San Diego (CA): Academic Press; p. 531–537.
Ford JKB, Ellis GM, Matkin CO, Wetklo MH, Barrett-Lennard LG, Withler RE. 2011. Shark predation and tooth wear in a population of northeastern Pacific killer whales. Aquat Biol. 11(3):213–224.
Fordyce RE. 2018. Cetacean Evolution. In: Würsig B, Thewissen JGM, Kovacs KM, editors. Encyclopedia of Marine Mammals (Third Edition). San Diego (CA): Academic Press; p. 180–185.
Galatius A, Racicot R, McGowen M, Olsen MT. 2020. Evolution and Diversification of Delphinid Skull Shapes. iScience. 23(10):101543. doi:10.1016/j.isci.2020.101543.
Gallagher WB. 2003. Oligotrophic oceans and minimalist organisms: collapse of the Maastrichtian marine ecosystem and Paleocene recovery in the Cretaceous-Tertiary sequence of New Jersey. Neth J Geosci. 82:225–231.
Hasegawa Y, Kimura T, Koda Y. 2006. Fossil physeterid from the Miocene Urizura Formation, Taga Group, Ibaraki, Japan. Bull Gunma Museum Nat Hist. 10:25–36.
Hassan MA, Westermann GEG, Hewitt RA, Dokainish MA. 2002. Finite-element analysis of simulated ammonoid septa (extinct Cephalopoda): septal and sutural complexities do not reduce strength. Paleobiology. 28(1):113–126.
Heithaus MR. 2001. Predator-prey and competitive interactions between sharks (order Selachii) and dolphins (suborder Odontoceti): a review. J Zool. 253 (1):53–68.
Herbert TD, Lawrence KT, Tzanova A, Peterson LC, Caballero-Gill R, Kelly CS. 2016. Late Miocene global cooling and the rise of modern ecosystems. Nat Geosci. 9(11):843–847.
Heupel MR, Knip DM, Simpfendorfer CA, Dulvy NK. 2014. Sizing up the ecological role of sharks as predators. Mar Ecol Prog Ser. 495:291–298.
Hocking DP, Marx FG, Park T, Fitzgerald EMG, Evans AR. 2017. A behavioural framework for the evolution of feeding in predatory aquatic mammals. P Roy Soc B. 284:20162750. doi:10.1098/rspb.2016.2750
Jouve S, Bouya B, Amaghzaz M. 2005. A short-snouted dyrosaurid (Crocodyliformes, Mesoeucrocodylia) from the Palaeocene of Morocco. Palaeontology. 48(2):359–369.
Kienle SS, Law CJ, Costa DP, Berta A, Mehta RS. 2017. Revisiting the behavioural framework of feeding in predatory aquatic mammals. P Roy Soc B. 284(1863):20171035. doi:10.1098/RSPB.2017.1035.
Kim SL, Tinker MT, Estes JA, Koch PL. 2012. Ontogenetic and among-individual variation in foraging strategies of northeast Pacific white sharks based on stable isotope analysis. PLoS One. 7(9):e45068. doi:10.1371/journal.pone.0045068.
Kimura T, Hasegawa Y, Barnes LG. 2006. Fossil sperm whales (Cetacea, Physeteridae) from Gunma and Ibaraki prefectures, Japan; with observations on the Miocene fossil sperm whale *Scaldicetus shigensis* Hirota and Barnes, 1995. Bull Gunma Museum Nat Hist. 10:1–23.
Kohler NE, Casey JG, Turner PA. 1996. Length-length and length-weight relationships for 13 shark species from the Western North Atlantic. In: NOAA Tech Rep Memo. NMMFS-NE. 110:1–22.
Koolstra JH, Tmgj VE, Weijs WA, Naeije M. 1988. A three-dimensional mathematical model of the human masticatory system predicting maximum possible bite forces. J Biomech. 21(7):563–576.
Lambert O. 2008. Sperm whales from the Miocene of the North Sea: a re-appraisal. Bull Inst R Sc N B. 78:277–316.
Lambert O, Bianucci G. 2019. How to break a sperm whale's teeth: dental damage in a large Miocene physeteroid from the North Sea Basin. J Vertebr Paleontol. 39(4):e1660987. doi:10.1080/02724634.2019.1660987.
Lambert O, Bianucci G, Beatty BL. 2014. Bony outgrowths on the jaws of an extinct sperm whale support macroraptorial feeding in several stem physeteroids. Naturwissenschaften. 101(6):517–521.
Lambert O, Bianucci G, De Muizon C. 2008. A new stem-sperm whale (Cetacea, Odontoceti, Physeteroidea) from the Latest Miocene of Peru. C R Palevol. 7 (6):361–369.
Lambert O, Bianucci G, De Muizon C. 2017. Macroraptorial sperm whales (cetacea, odontoceti, physeteroidea) from the Miocene of Peru. Zool J Linn Soc-Lond. 179(2):404–474.

Lambert O, Bianucci G, Post K, De Muizon C, Salas-Gismondi R, Urbina M, Reumer J. 2010. The giant bite of a new raptorial sperm whale from the Miocene epoch of Peru. Nature. 466(7302):105–108.
Lambert O, De Muizon C, Urbina M, Bianucci G. 2020. A new longirostrine sperm whale (Cetacea, Physeteroidea) from the lower Miocene of the Pisco Basin (southern coast of Peru). J Syst Palaeontol. 18(20):1707–1742.
Landini W, Altamirano-Sierra A, Collareta A, Di Celma C, Urbina M, Bianucci G. 2017. The late Miocene elasmobranch assemblage from Cerro Colorado (Pisco Formation, Peru). J S Am Earth Sci. 73:168–190
Loch C, Kieser JA, Fordyce RE. 2015. Enamel Ultrastructure in Fossil Cetaceans (Cetacea: archaeoceti and Odontoceti). PLoS One. 10(1):e0116557. doi:10.1371/JOURNAL.PONE.0116557.
Loch C, Swain MV, Van Vuuren LJ, Kieser JA, Fordyce RE. 2013. Mechanical properties of dental tissues in dolphins (Cetacea: delphinoidea and Inioidea). Arch Oral Biol. 58(7):773–779.
Loch C, van Vuuren LJ. 2016. Ultrastructure, biomechanical and chemical properties of the vestigial dentition of a Cuvier's beaked whale. New Zeal J Zool. 43(2):171–178.
Long DJ, Jones RE. 1996. White shark predation and scavenging on cetaceans in the eastern North Pacific Ocean. In: Klimley AP, Ainley DG, editors. Great White Sharks: the Biology of *Carcharodon carcharias*. San Diego (CA): Academic Press; p. 293–307.
Madzia D, Cau A. 2017. Inferring 'weak spots' in phylogenetic trees: application to mosasauroid nomenclature. PeerJ. 5(9):e3782. doi:10.7717/peerj.3782.
Mallison H, Wings O. 2014. Photogrammetry in paleontology-a practical guide. J Paleontol Tech. 12:1–31.
Marra AC, Carone G, Bianucci G. 2016. Sperm whale teeth from the late Miocene of Cessaniti (Southern Italy). Boll Soc Paleontol I. 55(3):223–225.
Martin RB, Burr DB, Sharkey NA, Fyhrie DP. 2015. Skeletal Tissue Mechanics. New York (NY): Springer New York.
Marx FG, Fordyce RE. 2015. Baleen boom and bust: a synthesis of mysticete phylogeny, diversity and disparity. R Soc Open Sci. 2:140434. doi:10.1098/rsos.140434
McCurry MR, Fitzgerald EMG, Evans AR, Adams JW, McHenry CR. 2017. Skull shape reflects prey size niche in toothed whales. Biol J Linn Soc. 121 (4):936–946.
McHenry CR. 2009. 'Devourer of Gods' The palaeoecology of the Cretaceous pliosaur *Kronosaurus queenslandicus* [dissertation]. Newcastle upon Tyne (NE): University of Newcastle.
McHenry CR, Wroe S, Clausen PD, Moreno K, Cunningham E. 2007. Supermodeled sabercat, predatory behavior in *Smilodon fatalis* revealed by high-resolution 3D computer simulation. Proc Natl Acad Sci USA. 104 (41):16010–16015.
Menesini E. 1969. Ittiodontoliti miocenici di Terra d'Otranto [Miocene ichthyodontolites from Terra d'Otranto]. Palaeontogr Ital. 65:1–61.
Morey G, Martìnez M, Massutì E, Moranta J. 2003. The occurrence of white sharks, *Carcharodon carcharias*, around the Balearic Islands (western Mediterranean Sea). Environ Biol Fish. 68(4):425–432.
Moro S, Jona-Lasinio G, Block B, Micheli F, De Leo G, Serena F, Bottaro M, Scacco U, Ferretti F. 2020. Abundance and distribution of the white shark in the Mediterranean Sea. Fish Fish. 21(2):338–349.
Notarbartolo di Sciara G. 2016. Chapter One - Marine Mammals in the Mediterranean Sea: an Overview. In: Notarbartolo Di Sciara G, Podestà M, Curry BE, editors. Mediterranean Marine Mammal Ecology and Conservation, Advances in Marine Biology 75. San Diego (CA): Academic Press; p. 1–36.
Notarbartolo di Sciara G, oMC V, Zanardelli M, Bearzi G, FJ B, Cavalloni B. 1993. Cetaceans in the central Mediterranean Sea: distribution and sighting frequencies. Ital J Zool. 60(1):131–138.
Notarbartolo di Sciara G, Reeves R 2006. The status and distribution of Cetaceans in the Black Sea and Mediterranean sea. Málaga; IUCN Centre for Mediterranean Cooperation, p. 142.
Oldfield CC, McHenry CR, Clausen PD, Chamoli U, Parr WCH, Stynder DD, Wroe S. 2012. Finite element analysis of ursid cranial mechanics and the prediction of feeding behaviour in the extinct giant *Agriotherium africanum*. J Zool. 286(2):171.
Perez VJ, Godfrey SJ, Kent BW, Weems RE, Nance JR. 2018. The transition between *Carcharocles chubutensis* and *Carcharocles megalodon* (Otodontidae, Chondrichthyes): lateral cusplet loss through time. J Vertebr Paleontol. 38(6): e1546732. doi:10.1080/02724634.2018.1546732.
Perez VJ, Leder RM, Badaut T. 2021. Body length estimation of Neogene macrophagous lamniform sharks (*Carcharodon* and *Otodus*) derived from associated fossil dentitions. Palaeontol Electron. 24(1):a09. doi:10.26879/1140.
Peri E, Collareta A, Bianucci G. 2020. A new record of physeteroidea from the upper Miocene of the pietra leccese (southern Italy): systematics, paleoecology and taphonomy of a fossil macroraptorial sperm whale. Riv Ital Paleontol S. 126(3):751–769.
Petti FM, Avanzini M, Belvedere M, De Gasperi M, Ferretti P, Girardi S, Remondino F, Tomasoni R. 2008. Digital 3D modelling of dinosaur footprints by photogrammetry and laser scanning techniques: integrated approach at the Coste dell'Anglone tracksite (Lower Jurassic, Southern Alps, Northern Italy). Studi Trent Sci Nat, Acta Geol. 83:303–315.
Piazza DS, Agnolin FL, Lucero S. 2018. First record of a macroraptorial sperm whale (Cetacea, Physeteroidea) from the Miocene of Argentina. Rev Bras Paleontolog. 21(3):276–280.
Pilleri G. 1970. Observation on the behavior of *Platanista gangetica* in the Indus and Brahmaputra rivers. Investig Cetacea. 2:27–60.
Pimiento C, Cantalapiedra JL, Shimada K, Field DJ, Smaers JB. 2019. Evolutionary pathways toward gigantism in sharks and rays. Evolution. 73 (3):588–599.
Pitman RL, Ballance LT, Mesnick SI, Chivers SJ. 2001. Killer whale predation on sperm whales: observations and implications. Mar Mammal Sci. 17 (3):494–507.
Pitman RL, Totterdell JA, Fearnbach H, Ballance LT, Durban JW, Kemps H. 2015. Whale killers: prevalence and ecological implications of killer whale predation on humpback whale calves off Western Australia. Mar Mammal Sci. 31:629–657. doi:10.1111/mms.12182
Polcyn MJ, Jacobs LL, Araújo R, Schulp AS, Mateus O. 2014. Physical drivers of mosasaur evolution. Palaeogeogr Palaeocl. 400:17–27.
Puértolas-Pascual E, Blanco A, Brochu CA, Canudo JI. 2015. Review of the late cretaceous-early Paleogene crocodylomorphs of Europe: extinction patterns across the K-Pg boundary. Cretaceous Res. 57:565–590.
Purdy RW, Schneider VP, Applegate SP, McLellan JH, Meyer RL, Slaughter BH. 2001. The Neogene sharks, rays, and bony fishes from Lee Creek Mine, Aurora, North Carolina. Sm C Paleob. 90:71–202.
Rayfield EJ, Milner AC, Xuan VB, Young PG. 2007. Functional morphology of spinosaur 'crocodile-mimic' dinosaurs. J Vertebr Paleontol. 27(4):892–901.
Rayfield EJ, Norman DB, Horner CC, Horner JR, Smith PM, Thomason JJ, Upchurch P. 2001. Cranial design and function in a large theropod dinosaur. Nature. 409(6823):1033–1037.
Read MA, Grigg GC, Irwin SR, Shanahan D, Franklin CE. 2007. Satellite tracking reveals long distance coastal travel and homing by translocated estuarine crocodiles, *Crocodylus porosus*. PLoS One. 2(9):e949.
Reumer JWF, Mens TH, Post K. 2017. New finds of giant raptorial sperm whale teeth (Cetacea, Physeteroidea) from the Westerschelde Estuary (province of Zeeland, the Netherlands). Deinsea. 17:32–38.
Rohr JJ, Fish FE. 2004. Strouhal numbers and optimization of swimming by odontocete cetaceans. J Exp Biol. 207(10):1633–1642.
Schaller GB. 2009. The Serengeti lion: a study of predator-prey relations. Chicago (IL): University of Chicago Press.
Seagars DJ. 1982. Jaw structure and functional mechanics of six delphinids (Cetacea: odontoceti). San Diego (CA): San Diego State University. master's thesis.
Shimada K, Becker MA, Griffiths ML. 2020. Body, jaw, and dentition lengths of macrophagous lamniform sharks, and body size evolution in Lamniformes with special reference to 'off-the-scale' gigantism of the megatooth shark, *Otodus megalodon*. Hist Biol. 1–17. doi:10.1080/08912963.2020.1812598
Simpfendorfer CA, Goodreid AB, Mcauley RB. 2001. Size, sex and geographic variation in the diet of the tiger shark, *Galeocerdo cuvier*, from Western Australian waters. Environ Biol Fish. 61(1):37–46.
Skomal GB, Braun CD, Chisholm JH, Thorrold SR. 2017. Movements of the white shark *Carcharodon carcharias* in the North Atlantic Ocean. Mar Ecol Prog Ser. 580:1–16.
Slater GJ, Goldbogen JA, Pyenson ND. 2017. Independent evolution of baleen whale gigantism linked to Plio-Pleistocene ocean dynamics. P Roy Soc B. 284:20170546. doi:10.1098/rspb.2017.0546
Snively E, Fahlke JM, Welsh RC. 2015. Bone-breaking bite force of *Basilosaurus isis* (Mammalia, Cetacea) from the late Eocene of Egypt estimated by finite element analysis. PLoS One. 10(2):e0118380. doi:10.1371/JOURNAL.PONE.0118380.
Sunquist M, Sunquist F. 2002. Wild Cats of the World. Chicago (IL): University of Chicago Press.
Tanner JB, Dumont ER, Sakai ST, Lundrigan BL, Holekamp KE. 2008. Of arcs and vaults: the biomechanics of bone-cracking in spotted hyenas (*Crocuta crocuta*). Biol J Linn Soc. 95(2):246–255.
Tanner T, Hernández-Almeida I, Drury AJ, Guitián J, Stoll H. 2020. Decreasing atmospheric CO2 during the late Miocene cooling. Paleoceanogr Paleoclimatology. 35(12):2020PA003925. doi:10.1029/2020PA003925.
Thomason JJ. 1991. Cranial strength in relation to estimated biting forces in some mammals. Can J Zool. 69(9):2326–2333.
Tubelli AA, Ketten DR. 2019. The role of material properties in cetacean hearing models: knowns and unknowns. Aquat Mamm. 45(6):717–732.

Uhen MD. 1996. *Dorudon atrox* (Mammalia, Cetacea): form, function, and phylogenetic relationships of an archaeocete from the late middle Eocene of Egypt [dissertation]. Ann Arbor (MI): University of Michigan.
Uhen MD. 2004. Form, function, and anatomy of *Dorudon atrox* (Mammalia, Cetacea): an archaeocete from the Middle to Late Eocene of Egypt. Pap Palaeontol. 34:1–238.
Uhen MD. 2018. Basilosaurids and Kekenodontids. In: Würsig B, Thewissen JGM, Kovacs KM, editors. Encyclopedia of Marine Mammals (Third Edition). San Diego (CA): Academic Press; p. 78–80.
Vescogni A, Vertino A, Bosellini FR, Harzhauser M, Mandic O. 2018. New paleoenvironmental insights on the Miocene condensed phosphatic layer of Salento (southern Italy) unlocked by the coral-mollusc fossil archive. Facies. 64(2):1–21.
Von Schulte HW, De Forest Smith M. 1918. The external characters, skeletal muscles, and peripheral nerves of *Kogia breviceps* (Blainville). B Am Mus Nat Hist. 38:7–72.
Voss M, Antar MSM, Zalmout IS, Gingerich PD. 2019. Stomach contents of the archaeocete *Basilosaurus isis*: apex predator in oceans of the late Eocene. PLoS One. 14(1):e0209021. doi:10.1371/JOURNAL.PONE.0209021.
Weijs WA, Hillen B. 1985. Cross-sectional areas and estimated intrinsic strength of the human jaw muscles. Acta Morphol Neer Sc. 23(3):267–274.
Werth AJ. 2000. Feeding in Marine Mammals. In: Schwenk K, editor. Feeding. San Diego (CA): Academic Press; p. 487–526.
Werth AJ. 2004. Functional Morphology of the Sperm Whale *Physeter macrocephalus* Tongue, with Reference to Suction Feeding. Aquat Mamm. 30(3):405–418.
Werth AJ. 2006a. Mandibular and dental variation and the evolution of suction feeding in odontoceti. J Mammal. 87(3):579–588.
Werth AJ. 2006b. Odontocete suction feeding: experimental analysis of water flow and head shape. J Morphol. 267(12):1415–1428.
Wroe S, Clausen P, McHenry C, Moreno K, Cunningham E. 2007. Computer simulation of feeding behaviour in the thylacine and dingo as a novel test for convergence and niche overlap. P Roy Soc B. 274 (1627):2819–2828.
Wroe S, Huber DR, Lowry M, McHenry C, Moreno K, Clausen P, Ferrara TL, Cunningham E, Dean MN, Summers AP. 2008. Three-dimensional computer analysis of white shark jaw mechanics: how hard can a great white bite? J Zool. 276(4):336–342.
Wroe S, McHenry C, Thomason J. 2005. Bite club: comparative bite force in big biting mammals and the prediction of predatory behaviour in fossil taxa. P Roy Soc B. 272(1563):619–625.
Yamato M, Ketten DR, Arruda J, Cramer S. 2008. Biomechanical and structural modeling of hearing in baleen whales. Bioacoustics. 17(1–3):100–102.